

Mechanically-exfoliated low-layered $[\text{Ca}_2\text{CoO}_3]_{0.62}[\text{CoO}_2]$: A single-crystalline p-type transparent conducting oxide

Reiji Okada,^{a)} Hiroto Isomura, Yoshiki J. Sato, Ryuji Okazaki, Masayuki Inoue, and Shinya Yoshioka
Department of Physics and Astronomy, Tokyo University of Science, Noda 278-8510, Japan

Transparent conducting oxides (TCOs) are essential components of optoelectronic devices and various materials have been explored for highly efficient TCOs having a combination of high transmittance and low sheet resistance. Here, we focus on a misfit thermoelectric oxide $[\text{Ca}_2\text{CoO}_3]_{0.62}[\text{CoO}_2]$ and fabricate the transparent low-layered crystals by a mechanical tape-peeling method using the single-crystalline samples. From the transmittance measurement, we find that the thickness of low-layered samples is several orders of hundred nanometers, which is comparable with the estimation from the scanning electron microscopy images. Compared to the previous results on the polycrystalline and *c*-axis oriented transparent films, the electrical resistivity is reduced owing to the single-crystalline nature. The figure of merit for the transparent conducting materials in the present low-layered samples is then evaluated to be higher than the values in the previous reports. The present results on the low-layered single-crystalline $[\text{Ca}_2\text{CoO}_3]_{0.62}[\text{CoO}_2]$ may offer a unique class of multi-functional transparent thermoelectric oxides.

Transparent conducting oxides (TCOs) show good electrical conductivity and optical transparency in the visible range, and are widely adopted as components of optoelectronic devices such as liquid crystal displays and touch screens¹⁻³. Among such TCOs, n-type materials including indium oxides⁴⁻⁸, zinc oxides⁹, tin oxides¹⁰, and titanium oxides¹¹ are known as highly efficient TCOs and have been often used as those components. On the other hand, p-type TCOs are less used due to their low carrier mobility^{12,13}, although various p-type TCOs such as NiO¹⁴, Cr₂O₃¹⁵, SrCu₂O₂¹⁶, LaCuOS¹⁷, delafossite series CuMO₂¹⁸⁻²³, V₂O₃^{24,25}, and perovskite oxides^{26,27} have been studied so far. The development of p-type TCOs including computational approach²⁸ is thus expected for future optoelectronic applications such as the growing field of the transparent semiconductors in which the p-n junction is essential²⁹⁻³¹.

Recently, misfit layered cobalt oxide $[\text{Ca}_2\text{CoO}_3]_{0.62}[\text{CoO}_2]$ thin films have been proposed as a peculiar class of p-type efficient TCOs. As shown in Fig. 1(a), the crystal structure of this material is two-dimensional, consisting of alternating rocksalt-type Ca_2CoO_3 block layers and CdI₂-type triangular-lattice CoO_2 conducting layers stacking along the *c* axis³²⁻³⁴. Interestingly, these two layers possess different lattice parameters along the *b*-axis direction to establish incommensurate nature as is also seen in layered chalcogenide materials³⁵. Thus, $\gamma = 0.62$ in $[\text{Ca}_2\text{CoO}_3]_{\gamma}[\text{CoO}_2]$ is approximate value for the incommensurate structure, and this material is often called $\text{Ca}_3\text{Co}_4\text{O}_9$ as the approximate chemical formula. $[\text{Ca}_2\text{CoO}_3]_{0.62}[\text{CoO}_2]$ has been intensively studied as an promising oxide thermoelectrics because of its large positive Seebeck coefficient of $S \approx 130 \mu\text{V/K}$ near room temperature owing to the entangled spin and orbital entropy of correlated Co 3d electrons, coexisting with the metallic resistivity³⁶⁻⁴⁰.

For the promising aspect of $[\text{Ca}_2\text{CoO}_3]_{0.62}[\text{CoO}_2]$ for

TCOs, Aksit *et al* and Fu *et al* have reported the optical transmittance and electrical transport measurements on the transparent polycrystalline⁴¹ and *c*-axis oriented⁴² thin films, respectively. The figure of merit (FOM) for TCOs has been evaluated as $-1/(R_{\text{sheet}} \times \ln T_{\text{opt}})$, where R_{sheet} is the sheet resistance and T_{opt} is the transmittance averaged for the specific photon energies in the visible range^{27,43}. Although the evaluated values of FOM ($151 \text{ M}\Omega^{-1}$ for the polycrystalline film⁴¹ and $988 \text{ M}\Omega^{-1}$ for the *c*-axis oriented film⁴²) are still less efficient, these previous studies suggest a potential layered optoelectronic oxides for the p-type TCOs.

In this paper, we attempt to fabricate transparent low-layered $[\text{Ca}_2\text{CoO}_3]_{0.62}[\text{CoO}_2]$ single crystals by utilizing a mechanical tape-peeling method. This simple peeling method may have a certain merit for the layered crystals to keep high carriers mobility⁴⁴. In this method, we have fabricated the transparent low-layered single crystals on the glass substrate with typical thickness of several orders of hundred nanometers. Through the transmittance and sheet resistance measurements, we find that the FOM of the present low-layered crystals is higher than the values reported in the previous studies. These results indicate that the present low-layered $[\text{Ca}_2\text{CoO}_3]_{0.62}[\text{CoO}_2]$ is not only a potential p-type TCO but also a unique class of transparent thermoelectric oxides with multi-functional properties.

We have first grown single-crystalline samples of $[\text{Ca}_2\text{CoO}_3]_{0.62}[\text{CoO}_2]$ by using a flux method⁴⁶⁻⁴⁸. The low-layered single crystals were fabricated by utilizing a tape peeling method. The single crystal was first sandwiched by the peeling tapes to remove the irregular surfaces of the crystal. Then, as illustrated in Figs. 1(b) and 1(c), the cleaved crystal was fixed on the glass substrate by using a small amount of transparent adhesive bond and mechanically exfoliated by the tape peeling method. The transparent low-layered region was partly obtained in the single crystal as shown in Fig. 1(e). Figure 1(f) displays a side-view scanning-electron-microscope (SEM) image for small pieces of the exfoliated crystals, indicating that the crystal thickness is approximately less than $1 \mu\text{m}$. The present fabrication of low-layered crystals is interesting because the layered coupling in $[\text{Ca}_2\text{CoO}_3]_{0.62}[\text{CoO}_2]$ may have rather strong covalent nature in contrast to the weak

^{a)}Authors to whom correspondence should be addressed: [Reiji Okada, 6222508@ed.tus.ac.jp; Yoshiki J. Sato, yoshiki_sato@rs.tus.ac.jp; Ryuji Okazaki, okazaki@rs.tus.ac.jp]

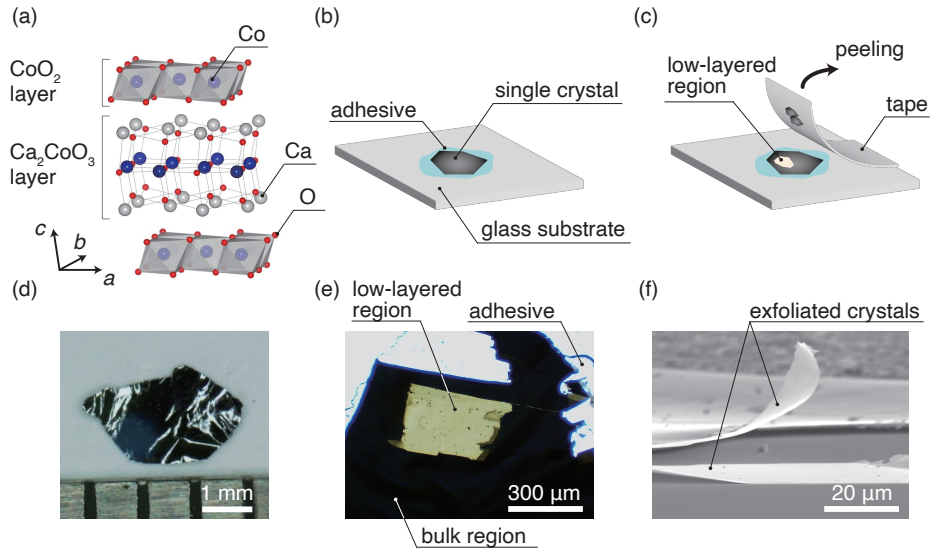


FIG. 1. Fabrication process of the low-layered $[\text{Ca}_2\text{CoO}_3]_{0.62}[\text{CoO}_2]$ single crystals. (a) Crystal structure of $[\text{Ca}_2\text{CoO}_3]_{0.62}[\text{CoO}_2]$ drawn by VESTA⁴⁵. (b) Schematic diagram of the fabrication process. Thin crystal is fixed on a glass substrate by using an adhesive bond. (c) The low-layered crystal is partly obtained by a tape-peeling method. (d) Photograph of the bulk single crystal grown by the flux method. (e) Photograph of the mechanically-exfoliated single crystal. Transparent yellow-colored area is the mechanically-exfoliated low-layered region of the crystal. (f) Side-view SEM image for the small pieces of the mechanically-exfoliated single crystal.

interlayer coupling of van der Waals materials. Owing to the incommensurate layered structure of $[\text{Ca}_2\text{CoO}_3]_{0.62}[\text{CoO}_2]$, the samples may become more exfoliative to realize such transparent low-layered crystals. Note that similar layered cobalt oxide $\text{Bi}_2\text{Sr}_2\text{Co}_2\text{O}_8$ could be exfoliated into nanosheets due to weak van der Waals interlayer coupling^{49–51}.

The transmittance spectra were measured by using a USB module of a complementary metal-oxide semiconductor (CMOS) spectrometer equipped with an optical microscope. We evaluated the transmittance $T(\omega)$ as $T(\omega) = I_{\text{sample}}(\omega)/I_{\text{ref}}(\omega)$, where $I_{\text{sample}}(\omega)$ is the intensity spectrum for the low-layered crystal on the glass substrate and $I_{\text{ref}}(\omega)$ is the reference spectrum for the glass substrate without samples. To consider the reflection at the interfaces, the absorbance was obtained as follows: The measured intensity I_{sample} is given as $I_{\text{sample}} = I_0(1 - R_1)(1 - R_2)e^{-\alpha d}$, where I_0 is the intensity of incident light, R_1 and R_2 are the reflectance at the crystal-glass and the crystal-air interfaces, respectively, and α is the absorption coefficient of the crystal. Note that the multiple reflection is negligibly small. Also, the reference intensity I_{ref} is given as $I_{\text{ref}} = I_0(1 - R_3)$, where R_3 is the reflectance at the glass-air interface. The measured transmittance T is then given as $T = I_{\text{sample}}/I_{\text{ref}} = e^{-\alpha d}/\gamma$, where $\gamma = \frac{1-R_3}{(1-R_1)(1-R_2)}$. According to Fresnel's equation, the interface reflection between the media α and β is calculated as $|(\tilde{n}_\alpha - \tilde{n}_\beta)/(\tilde{n}_\alpha + \tilde{n}_\beta)|^2$, where \tilde{n}_α and \tilde{n}_β are the complex refractive indices of the media α and β , respectively. We used $\tilde{n}_{\text{air}} = 1.0$ and $\tilde{n}_{\text{glass}} = 1.5$. The complex refractive index of the crystal $\tilde{n}_{\text{crystal}} = n(\omega) + i\kappa(\omega)$ is obtained from the Kramers-Kronig (KK) analysis⁵², where $n(\omega)$ is the refractive index and $\kappa(\omega)$ is the extinction coefficient. The absorbance of the crystal is then calculated from the measured

transmittance T as $A_{\text{exp}} = \alpha d \log_{10} e = -\log_{10}(\gamma T)$.

The sheet resistance R_{sheet} of the low-layered crystals was measured by using a conventional van der Pauw method. The excitation current of $I = 10 \mu\text{A}$ was applied by Keithley 6221 current source and the voltage was measured with synchronized Keithley 2182A nanovoltmeter. These two instruments were operated in a built-in Delta mode to cancel the offset voltage. We used a closed refrigerator to evaluate the temperature dependence of the sheet resistance below room temperature.

Figure 2(a) depicts the transmittance spectra $T(\omega)$ of the low-layered $[\text{Ca}_2\text{CoO}_3]_{0.62}[\text{CoO}_2]$ single crystals in the visible range. The inset of Fig. 2(a) shows the optical image of the measured sample and the measured area is indicated by the red rectangular. The measured low-layered region is yellow-colored transparent and the averaged transmittance in the visible range is about 0.3, indicating that thin low-layered crystal is fabricated in the present peeling process using single crystals.

To estimate the thickness of the low-layered crystals, we now consider the absorbance of the crystal. As described before, we evaluate the absorbance spectra of the low-layered crystals $A_{\text{exp}}(\omega)$ from the measured transmittance $T(\omega)$. The absorbance spectra of typical low-layered crystal $A_{\text{exp}}(\omega)$ is shown in Fig. 2(b) with the red curve. Then, we also calculate the absorbance spectra $A_{\text{calc}}(\omega)$ from the reflectivity data in the previous study⁵². Using the extinction coefficient $\kappa(\omega)$ obtained by the KK analysis, we calculate $A_{\text{calc}}(\omega)$ for several values of the sample thickness d as

$$A_{\text{calc}}(\omega) = \frac{1}{\ln 10} \frac{2\omega\kappa(\omega)}{c} d, \quad (1)$$

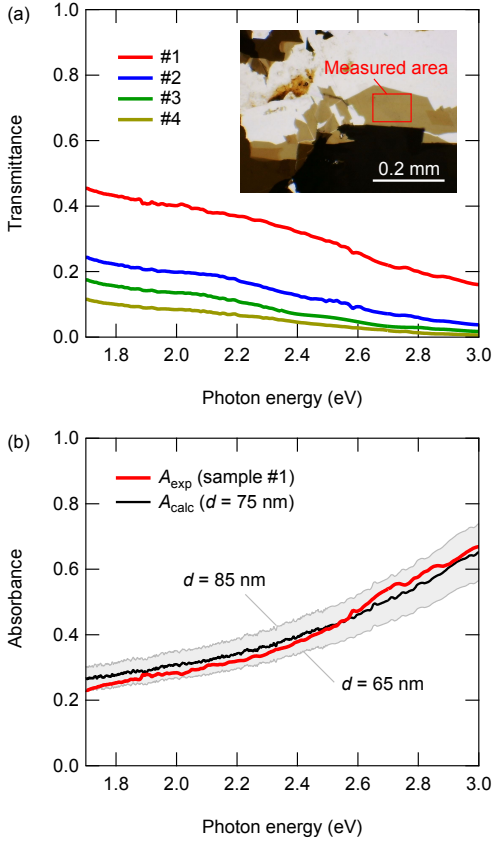


FIG. 2. (a) Transmittance spectra of the low-layered $[\text{Ca}_2\text{CoO}_3]_{0.62}[\text{CoO}_2]$ single crystals. The inset shows the photograph of the measure crystal and the red rectangular indicates the measured area for the transmittance spectra. (b) Absorbance spectra. In the present study, we compare the absorbance spectra obtained from the present transmittance measurements, A_{exp} , with the calculated data A_{calc} from the earlier optical study by assuming several values of the sample thickness d . See text for details.

where c is the speed of light. In Fig. 2(b), we also plot $A_{\text{calc}}(\omega)$ for several values of d , and $A_{\text{calc}}(\omega)$ data calculated with $d = 75$ nm is matched with $A_{\text{exp}}(\omega)$ data measured in the present study, indicating that the thickness of the present low-layered crystal is $d \approx 75$ nm and the uncertainty is approximately 10 nm. We evaluate the thickness of several crystals in the same manner, and typical value of the thickness is found to be a few hundred nanometers, consistent with the SEM image for the side view of low-layered crystals shown in Fig. 1(f).

To examine the sheet resistance of the low-layered transparent single crystals, we have prepared a rectangular-shaped low-layered sample by cutting the exfoliated crystal and made four electrical contacts at the corners by using a silver paint as shown in the inset of Fig. 3(a). The sheet resistance R_{sheet} is then measured by the conventional van der Pauw (vdP) method, and the obtained temperature dependence of R_{sheet} and the resistivity $\rho = R_{\text{sheet}} \times d$ are shown in Figs. 3(a) and 3(b), respectively. Note that the measured resistivity in the vdP configuration is given as the geometric mean

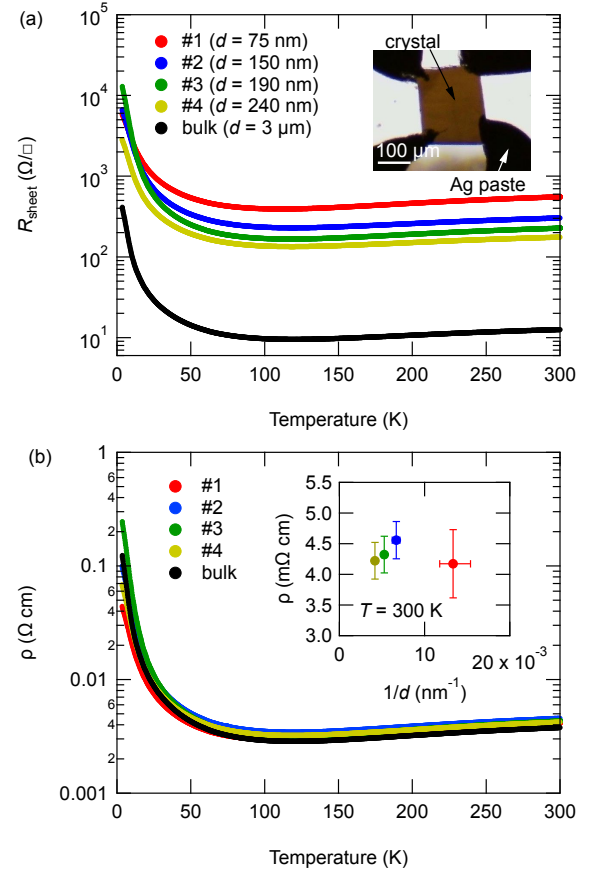


FIG. 3. (a) Temperature dependence of the sheet resistance R_{sheet} obtained by the van der Pauw method. The inset shows a photograph of the low-layered rectangular-shaped sample attached with four electrical contacts at the corners. (b) Temperature dependence of the resistivity ρ evaluated as $\rho = R_{\text{sheet}} \times d$. The inset shows the the resistivity measured at 300 K as a function of the inverse of the thickness, $1/d$, for four low-layered crystals.

of $\rho = \sqrt{\rho_a \rho_b}$, where ρ_i ($i = a, b$) is the resistivity measured along i direction⁵³, since this material exhibits slight in-plane transport anisotropy⁵⁴.

Overall behavior of the temperature dependence of the resistivity in the present low-layered crystals agrees well with the previous data^{55,56}; near room temperature, a metallic resistivity of $\rho \approx 4$ m Ω cm is achieved and a semiconducting temperature dependence is observed below 100 K owing to the carrier localization effect⁵⁷ or a pseudo-gap formation associated with the spin-density-wave ordering⁵⁸. Thus, these results indicate that a single-crystalline transparent conducting oxide is well fabricated in the layered $[\text{Ca}_2\text{CoO}_3]_{0.62}[\text{CoO}_2]$ with no significant damage in the peeling process. Note that the low-temperature behavior seems sample-dependent, which probably comes from extrinsic effects such as the oxygen defects.

Generally, the resistivity of metallic films depends on the thickness due to the surface scattering as discussed in the Fuchs-Sondheimer model⁵⁹. In such case, the resistivity may

Samples	No.	d (nm)	R_{sheet} (Ω/\square)	ρ ($m\Omega\text{cm}$)	T_{opt} (%)	FOM ($M\Omega^{-1}$)	References
Low-layered single crystals	#1	75(10)	556	4.2(6)	31.1	1540	Present study
	#2	150(10)	304	4.6(3)	13.4	1637	
	#3	190(15)	227	4.3(3)	8.4	1779	
	#4	240(15)	176	4.2(3)	5.2	1922	
Polycrystalline film		100	5700	57	31.3	151	41
c -axis oriented film		50	1460	7.3	50	988	42

TABLE I. The room-temperature optoelectronic properties and the figure of merit (FOM) of transparent $[\text{Ca}_2\text{CoO}_3]_{0.62}[\text{CoO}_2]$ in various forms.

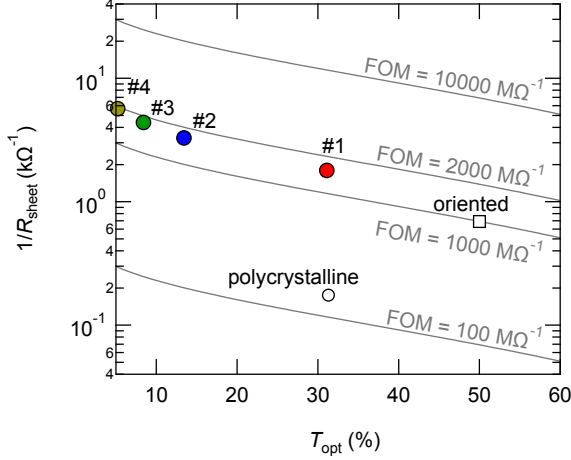


FIG. 4. Single logarithmic plot of the inverse sheet resistance $1/R_{\text{sheet}}$ vs the transmittance averaged for specific photon energies T_{opt} for various forms of $[\text{Ca}_2\text{CoO}_3]_{0.62}[\text{CoO}_2]$. The data for the polycrystalline and the c -axis oriented films are taken from Refs. 41 and 42, respectively. Solid curves represent the calculated curves for several values of FOM.

show a linear dependence of $\rho = \rho_0(1 + \Lambda/d)$, where ρ_0 and Λ are the bulk-crystal resistivity and a characteristic length, respectively. The characteristic length Λ is comparable to a mean free path of carriers near surfaces. We then plot the resistivity measured at 300 K as a function of the inverse of the thickness, $1/d$, for the low-layered crystals in the inset of Fig. 3(b), and find no significant thickness dependence. This result is consistent with the fact that the mean free path of $[\text{Ca}_2\text{CoO}_3]_{0.62}[\text{CoO}_2]$ is about 1 nm^{58} , which is much smaller than the thickness of the low-layered crystals, and indicates that the surface scattering is not dominant in the present case. On the other hand, a thickness-dependent metal-insulator transition has been observed in the nanosheets $\text{Bi}_2\text{Sr}_2\text{Co}_2\text{O}_8^{50}$, implying a strong thickness dependence of the resistivity in the layered oxides. Also, interesting spin-related surface transport⁶⁰ and two-dimensional quantum confinement effect⁶¹ have been suggested for the resistive behavior in the metallic films. A more detailed consideration may be required as a future study along with further magneto-transport experiments on the thinner low-layered crystals.

Having the observed transmittance and the sheet resistance, we now discuss the figure of merit (FOM) of the low-layered $[\text{Ca}_2\text{CoO}_3]_{0.62}[\text{CoO}_2]$ single crystals. The FOM for TCOs has

been evaluated with two different procedures²⁷: one is proposed by Haacke as $\text{FOM}^H = T_{\text{opt}}^{10}/R_{\text{sheet}}$, where R_{sheet} is the sheet resistance and T_{opt} is the transmittance averaged for specific photon energies ($\hbar\omega = 1.77, 2.0, 2.25, 2.5, 2.75, 3.0 \text{ eV}$). This evaluation however tends to overweight the importance of the transparency. The other is widely used one proposed by Gordon as

$$\text{FOM}^G = -\frac{1}{R_{\text{sheet}} \times \ln T_{\text{opt}}}, \quad (2)$$

which is also expressed as $\text{FOM}^G = \sigma/\alpha$ by using the electrical conductivity $\sigma = 1/(R_{\text{sheet}}d)$ and the absorption coefficient $\alpha \approx -(1/d)\ln T_{\text{opt}}$. Since FOM^G is evaluated in the earlier works on this material, we also use FOM^G as the figure of merit in this paper.

Table I summarizes the optoelectronic properties and the FOM of transparent $[\text{Ca}_2\text{CoO}_3]_{0.62}[\text{CoO}_2]$ in the present study and previous reports^{41,42}. Owing to the single-crystalline nature, the resistivity is lower than those in the previous reports^{41,42,62}, leading to large values of FOM. Note that the resistivity of the high-quality epitaxial films is comparable to that in the low-layered crystals⁵⁵ while the transmittance of the epitaxial films has not been evaluated. We also note that the FOM values slightly decrease with decreasing thickness: As mentioned previously, the measured transmittance is $T = e^{-ad}/\gamma$. Thus, using the conductivity $\sigma = 1/(R_{\text{sheet}}d)$, the FOM is given as $\text{FOM} = \sigma/(\alpha + \frac{1}{d}\ln\gamma)$. Since σ and α are thickness-independent parameters in principle and γ is larger than unity, this equation may indicate that the FOM value decreases with decreasing d owing to the reflectance at the interfaces in the present devices. Nonetheless, the FOM value in the present study is the same order of those in high-performance p -type TCOs such as $\text{CuCr}_{1-x}\text{Mg}_x\text{O}_2$ ($\text{FOM} \sim 5000 \text{ M}\Omega^{-1}$)²⁰ and $\text{La}_{2/3}\text{Sr}_{1/3}\text{VO}_3$ ($\text{FOM} \sim 7000 \text{ M}\Omega^{-1}$)²⁷. We note that doping effect such as Bi substitution⁵⁸ may be promising to further enhance the FOM in the low-layered $[\text{Ca}_2\text{CoO}_3]_{0.62}[\text{CoO}_2]$. Figure 4 represents the single logarithmic plot of the sheet conductance $1/R_{\text{sheet}}$ as a function of T_{opt} . In Fig. 4, we plot the room-temperature data for four low-layered single crystals as well as the data from an earlier study of the polycrystalline and the c -axis oriented films^{41,42}, along with the calculated curves for several values of FOM. Indeed, the present low-layered crystals exhibit higher value of FOM compared to those in previous study, indicating that the present peeling technique using single crystals is efficient certainly to realize high-performance TCOs.

To summarize, we have fabricated the transparent low-layered $[\text{Ca}_2\text{CoO}_3]_{0.62}[\text{CoO}_2]$ single crystals on the glass sub-

strate by utilizing mechanical peeling method. From the results of the optical and transport measurements, we find that the figure of merit in the present crystals is higher than the values reported in the previous studies on the polycrystalline and *c*-axis oriented films owing to the lower resistivity in the single-crystalline samples. Since $[\text{Ca}_2\text{CoO}_3]_{0.62}[\text{CoO}_2]$ has been studied as a potential oxide thermoelectrics, the present study offers a unique class of transparent thermoelectric oxides with multi-functional properties^{63,64}. Also, the present low-layered crystals belonging to the strongly correlated electrons system may provide a fascinating playground to investigate the nature of correlated electrons confined in low dimension.

Conflict of Interest

The authors have no conflicts to disclose.

DATA AVAILABILITY

The data that support the findings of this study are available from the corresponding author (R. Okazaki) upon reasonable request.

ACKNOWLEDGMENTS

We appreciate K. Tanabe for providing us with the reflectivity data of $[\text{Ca}_2\text{CoO}_3]_{0.62}[\text{CoO}_2]$ single crystals. This work was supported by JSPS KAKENHI Grant No. 22H01166 and Research Foundation for the Electrotechnology of Chubu (REFEC).

- ¹T. Minami, Transparent conducting oxide semiconductors for transparent electrodes. *Semicond. Sci. Technol.* **20**, S35 (2005).
- ²A. Stadler, Transparent Conducting Oxides-An Up-To-Date Overview. *Materials*, **5**, 661-683 (2012).
- ³S. C. Dixon, D. O. Scanlon, C. J. Carmalt and I. P. Parkin, N-Type doped transparent conducting binary oxides: an overview. *J. Mater. Chem. C* **4**, 6946-6961 (2016).
- ⁴I. Hamberg and C. G. Granqvist, Evaporated Sn-doped In_2O_3 films: Basic optical properties and applications to energy-efficient windows. *J. Appl. Phys.* **60**, R123-R160 (1986).
- ⁵J. M. Phillips, J. Kwo, G.A. Thomas, S. A. Carter, R. J. Cava, S. Y. Hou, J. J. Krajewski, J. H. Marshall, W. F. Peck, D. H. Rapkine, and R. B. van Dover, Transparent conducting thin films of GaInO_3 . *Appl. Phys. Lett.* **65**, 115-117 (1994).
- ⁶J. M. Phillips, R. J. Cava, G. A. Thomas, S. A. Carter, J. Kwo, T. Siegrist, J. J. Krajewski, J. H. Marshall, W. F. Peck, Jr., and D. H. Rapkine, Zinc-indium-oxide: A high conductivity transparent conducting oxide. *Appl. Phys. Lett.* **67**, 2246 (1995).
- ⁷R. B. H. Tahar, T. Ban, Y. Ohya, and Y. Takahashi, Tin doped indium oxide thin films: Electrical properties. *J. Appl. Phys.* **83**, 2631 (1998).
- ⁸Y. Meng, X. Yang, H. Chen, J. Shen, Y. Jiang, Z. Zhang and Z. Hua, A new transparent conductive thin film $\text{In}_2\text{O}_3:\text{Mo}$. *Thin Solid Films*, **394**, 219-223 (2001).
- ⁹A. Yamada, B. Sang, M. Konagai, Atomic layer deposition of ZnO transparent conducting oxides. *Appl. Surf. Sci.* **112**, 216-222 (1997).
- ¹⁰Y. Wang, T. Brezesinski, M. Antonietti, and B. Smarsly, Ordered mesoporous Sb-, Nb-, and Ta-doped SnO_2 thin films with adjustable doping levels and high electrical conductivity. *ACS Nano* **3**, 1373-1378 (2009).
- ¹¹T. Hitosugi, N. Yamada, S. Nakao, Y. Hirose, and T. Hasegawa, Properties of TiO_2 -based transparent conducting oxides. *Phys. Status Solidi A* **207**, 1529-1537 (2010).
- ¹²H. Ohta and H. Hosono, Transparent oxide optoelectronics. *Mater. Today* **7**, 42-51 (2004).
- ¹³K. H. L. Zhang, K. Xi, M. G. Blamire, and R. G. Egdell, P-type transparent conducting oxides. *J. Phys.: Condens. Matter* **28**, 383002 (2016).
- ¹⁴H. Sato, T. Minami, S. Tanaka, and T. Yamada, Transparent conducting p-type NiO thin films prepared by magnetron sputtering. *Thin Solid Films*. **236**, 27-31 (1993).
- ¹⁵N. Uekawa and K. Kaneko, Dopant Reduction in p-type Oxide Films upon Oxygen Absorption. *J. Phys. Chem.* **100**, 4193-4198 (1996).
- ¹⁶A. Kudo, H. Yanagi, H. Hosono, and H. Kawazoe, SrCu_2O_2 : A p-type conductive oxide with wide band gap. *Appl. Phys. Lett.* **73**, 220 (1998).
- ¹⁷K. Ueda, S. Inoue, S. Hirose, H. Kawazoe, and H. Hosono, Transparent p-type semiconductor: LaCuOS layered oxysulfide. *Appl. Phys. Lett.* **77**, 2701 (2000).
- ¹⁸H. Kawazoe, M. Yasukawa, H. Hyodo, M. Kurita, H. Yanagi, and H. Hosono, P-type electrical conduction in transparent thin films of CuAlO_2 . *Nature* **389**, 939-942 (1997).
- ¹⁹N. Duan, A. W. Sleight, M. K. Jayaraj, and J. Tate, Transparent p-type conducting CuScO_{2+x} films. *Appl. Phys. Lett.* **77**, 1325 (2000).
- ²⁰R. Nagarajan, A. D. Draeseke, A. W. Sleight, and J. Tate, P-type conductivity in $\text{CuCr}_{1-x}\text{Mg}_x\text{O}_2$ films and powders. *J. Appl. Phys.* **89**, 8022 (2001).
- ²¹H. Yanagi, T. Hase, S. Ibuki, K. Ueda, and H. Hosono, Bipolarity in electrical conduction of transparent oxide semiconductor CuInO_2 with delafossite structure. *Appl. Phys. Lett.* **78**, 1583 (2001).
- ²²M. K. Jayaraj, A. D. Draeseke, J. Tate, and A. W. Sleight, P-Type transparent thin films of $\text{CuY}_{1-x}\text{Ca}_x\text{O}_2$. *Thin Solid Films*. **397** 244-248 (2001).
- ²³M. Snure and A. Tiwari, CuBO_2 : A p-type transparent oxide. *Appl. Phys. Lett.* **91**, 092123 (2007).
- ²⁴L. Hu, M. L. Zhao, S. Liang, D. P. Song, R. H. Wei, X. W. Tang, W. H. Song, J. M. Dai, G. He, C. J. Zhang, X. B. Zhu, and Y. P. Sun, Exploring High-performance p-type Transparent Conducting Oxides based on Electron Correlation in V_2O_3 Thin Films. *Phys. Rev. Appl.* **12**, 044035 (2019).
- ²⁵M. Zhu, G. D. Zhang, D. P. Song, J. Y. Wu, R. R. Zhang, L. Hu, R. H. Wei, W. H. Song, X. B. Zhu, and Y. P. Sun, Enhancing the performances of V_2O_3 thin films as p-type transparent conducting oxides via compressive strain. *Appl. Phys. Lett.* **121**, 061903 (2022).
- ²⁶K. H. L. Zhang, Y. G. Du, A. Papadogianni, O. Bierwagen, S. Sallis, L. F. J. Piper, M. E. Bowden, V. Shutthanandan, P. V. Sushko, and S. A. Chambers, Perovskite Sr-Doped LaCrO_3 as a New p-Type Transparent Conducting Oxide. *Adv. Mater.* **27**, 5191 (2015).
- ²⁷L. Hu, R. Wei, J. Yan, D. Wang, X. Tang, X. Luo, W. Song, J. Dai, X. Zhu, C. Zhang, and Y. Sun, $\text{La}_{2/3}\text{Sr}_{1/3}\text{VO}_3$ Thin Films: A New p-Type Transparent Conducting Oxide with Very High Figure of Merit. *Adv. Electron. Mater.* **4**, 1700476 (2018).
- ²⁸G. Brunin, F. Ricci, V.-A. Ha, G.-M. Rignanese, and G. Hautier, Transparent conducting materials discovery using high-throughput computing. *npj Computational Materials* **5**, 63 (2019).
- ²⁹M.-J. Choi, M.-H. Kim, and D.-K. Choi, A transparent diode with high rectifying ratio using amorphous indium-gallium-zinc oxide/ SiN_x coupled junction. *Appl. Phys. Lett.* **107**, 053501 (2015).
- ³⁰H. Park, D. S. Oh, K. J. Lee, D. Y. Jung, S. Lee, S. Yoo, and S.-Y. Choi, Flexible and Transparent Thin-Film Transistors Based on Two-Dimensional Materials for Active-Matrix Display. *ACS Appl. Mater. Interfaces* **12**, 4749-4754 (2020).
- ³¹L. Hu, R. H. Wei, X. W. Tang, W. J. Lu, X. B. Zhu, and Y. P. Sun, Design strategy for p-type transparent conducting oxides. *J. Appl. Phys.* **128**, 140902 (2020);
- ³²A. Masset, C. Michel, A. Maignan, M. Hervieu, O. Toulemonde, F. Studer, and B. Raveau, Misfit-layered cobaltite with an anisotropic giant magnetoresistance: $\text{Ca}_3\text{Co}_4\text{O}_9$. *Phys. Rev. B* **62**, 166 (2000).
- ³³Y. Miyazaki, M. Onoda, T. Oku, M. Kikuchi, Y. Ishii, Y. Ono, Y. Morii, and T. Kajitani, Modulated Structure of the Thermoelectric Compound $[\text{Ca}_2\text{CoO}_3]_{0.62}\text{CoO}_2$. *J. Phys. Soc. Jpn.* **71**, 491 (2002).
- ³⁴M. Shikano and R. Funahashi, Electrical and thermal properties of single-crystalline $(\text{Ca}_2\text{CoO}_3)_{0.7}\text{CoO}_2$ with a $\text{Ca}_3\text{Co}_4\text{O}_9$ structure. *Appl. Phys. Lett.* **82**, 1851 (2003).

- ³⁵J. Rouxel, A. Meerschaut, and G. A. Wiegers, Chalcogenide misfit layer compounds. *J. Alloys Compd.* **229**, 144 (1995).
- ³⁶W. Koshibae, K. Tsutsui, and S. Maekawa, Thermopower in cobalt oxides. *Phys. Rev. B* **62**, 6869 (2000).
- ³⁷R. F. Klie, Q. Qiao, T. Paulauskas, A. Gulec, A. Rebola, S. Ögüt, M. P. Prange, J. C. Idrobo, S. T. Pantelides, S. Kolesnik, B. Dabrowski, M. Ozdemir, C. Boyraz, D. Mazumdar, and A. Gupta, Observations of Co^{4+} in a Higher Spin State and the Increase in the Seebeck Coefficient of Thermoelectric $\text{Ca}_3\text{Co}_4\text{O}_9$. *Phys. Rev. Lett.* **108**, 196601 (2012).
- ³⁸J. Hejtmánek, Z. Jirák, and J. Šebek, Spin-entropy contribution to thermopower in the $[\text{Ca}_2\text{CoO}_{3-x}]_{0.62}(\text{CoO}_2)$ misfits. *Phys. Rev. B* **92**, 125106 (2015).
- ³⁹S. Hébert, D. Berthebaud, R. Daou, Y. Bréard, D. Pelloquin, E. Guilmeau, F. Gascoin, O. Lebedev, and A. Maignan, Searching for new thermoelectric materials: some examples among oxides, sulfides and selenides. *J. Phys.: Condens. Matter* **28**, 013001 (2016).
- ⁴⁰Y. Yin, F. Shi, G.-Q. Liu, A. Tiwari, J. Hao, L. He, D. Liu, J. Cai, X. Tan, J. Jiang, B. Shen, Magnetic field enhanced thermal conductivity and origin of large thermopower in layered cobaltates. *J. Materomics* (2023) <https://doi.org/10.1016/j.jmat.2023.04.002>
- ⁴¹M. Aksit, S. K. Kolli, I. M. Slauch, R. D. Robinson, Misfit layered $\text{Ca}_3\text{Co}_4\text{O}_9$ as a high figure of merit p-type transparent conducting oxide film through solution processing. *Appl. Phys. Lett.* **104**, 161901 (2014).
- ⁴²G. Fu, G. Yan, L. Sun, H. Zhang, H. Guo, J. Wang and S. Wang, Enhanced transparent conducting performance of c-axis oriented $\text{Ca}_3\text{Co}_4\text{O}_9$ thin film. *RSC Adv.* **5**, 26383 (2015).
- ⁴³E. Arca, K. Fleischer, and I. V. Shvets, Magnesium, nitrogen codoped Cr_2O_3 : A p-type transparent conducting oxide. *Appl. Phys. Lett.* **99**, 111910 (2011).
- ⁴⁴K. S. Novoselov, A. K. Geim, S. V. Morozov, D. Jiang, Y. Zhang, S. V. Dubonos, I. V. Grigorieva, and A. A. Firsov, Electric Field Effect in Atomically Thin Carbon Films. *Science* **306**, 666-669 (2004).
- ⁴⁵K. Momma and F. Izumi, VESTA 3 for three-dimensional visualization of crystal, volumetric and morphology data. *J. Appl. Crystallogr.* **44**, 1272 (2011).
- ⁴⁶M. Mikami, K. Chong, Y. Miyazaki, T. Kajitani, T. Inoue, S. Sodeoka, and R. Funahashi, Bi-Substitution Effects on Crystal Structure and Thermoelectric Properties of $\text{Ca}_3\text{Co}_4\text{O}_9$ Single Crystals. *J. Appl. Phys.* **45**, 4131 (2006).
- ⁴⁷Y. Ikeda, K. Saito, and R. Okazaki, Thermoelectric transport in the layered $\text{Ca}_3\text{Co}_{4-x}\text{Rh}_x\text{O}_9$ single crystals. *J. Appl. Phys.* **119**, 225105 (2016).
- ⁴⁸K. Saito and R. Okazaki, Electron correlation effect in the thermoelectric oxide $\text{Ca}_{3-x}\text{Sr}_x\text{Co}_4\text{O}_9$ single crystals. *Jpn. J. Appl. Phys.* **56**, 043201 (2017).
- ⁴⁹W. J. Yu, Z. Li, H. Zhou, Y. Chen, Y. Wang, Y. Huang, and X. Duan, Vertically stacked multi-heterostructures of layered materials for logic transistors and complementary inverters *Nat. Mater.* **12**, 246 (2013).
- ⁵⁰Y. Wang, R. Cheng, J. Dong, Y. Liu, H. Zhou, W. J. Yu, I. Terasaki, Y. Huang, and X. Duan, Metal-semiconductor transition in atomically thin $\text{Bi}_2\text{Sr}_2\text{Co}_2\text{O}_8$ nanosheets. *APL Mater.* **2**, 092507 (2014).
- ⁵¹L. Li, X.-J. Yan, S.-T. Dong, Y.-Y. Lv, X. Li, S.-H. Yao, Y.-B. Chen, S.-T. Zhang, J. Zhou, H. Lu, M.-H. Lu, and Y.-F. Chen, Ultra-low thermal conductivities along c-axis of naturally misfit layered $\text{Bi}_2[\text{AE}]_2\text{Co}_2\text{O}_9$ (AE = Ca, $\text{Ca}_{0.5}\text{Sr}_{0.5}$, Sr, Ba) single crystals. *Appl. Phys. Lett.* **111**, 033902 (2017).
- ⁵²K. Tanabe, R. Okazaki, H. Taniguchi, and I. Terasaki, Optical conductivity of layered calcium cobaltate $\text{Ca}_3\text{Co}_4\text{O}_9$. *J. Phys. Condens. Matter* **28**, 085601 (2016).
- ⁵³L. J. van der Pauw, Determination of resistivity tensor and Hall tensor of anisotropic conductors. *Philips Res. Repts.* **16**, 187 (1961).
- ⁵⁴H. Sakabayashi and R. Okazaki, Crossover from itinerant to localized states in the thermoelectric oxide $[\text{Ca}_2\text{CoO}_3]_{0.62}[\text{CoO}_2]$. *Phys. Rev. B* **103**, 125119 (2021).
- ⁵⁵K. Sugiura, H. Ohta, K. Nomura, T. Saito, Y. Ikuhara, M. Hirano, H. Hosono, and K. Koumoto, Thermoelectric Properties of the Layered Cobaltite $\text{Ca}_3\text{Co}_4\text{O}_9$ Epitaxial Films Fabricated by Topotactic Ion-Exchange Method. *Mater. Trans.* **48**, 2104 (2007).
- ⁵⁶N. Murashige, F. Takei, K. Saito, and R. Okazaki, Nonlinear transport associated with spin density wave dynamics in $\text{Ca}_3\text{Co}_4\text{O}_9$. *Phys. Rev. B* **96**, 035126 (2017).
- ⁵⁷A. Bhaskar, Z.-R. Lin, and C.-J. Liu, Low-temperature thermoelectric and magnetic properties of $\text{Ca}_{3-x}\text{Bi}_x\text{Co}_4\text{O}_{9+\delta}$ ($0 \leq x \leq 0.30$). *J. Mater. Sci.* **49**, 1359 (2014).
- ⁵⁸Y.-C. Hsieh, R. Okazaki, H. Taniguchi, I. Terasaki, Pseudogap Observed in the Charge Transport in the Thermoelectric Oxide $\text{Ca}_{3-x}\text{Bi}_x\text{Co}_4\text{O}_9$ Single Crystals, *J. Phys. Soc. Jpn.* **83**, 054710 (2014).
- ⁵⁹J. S. Chawla, F. Gstrein, K. P. O'Brien, J. S. Clarke, and D. Gall, Electron scattering at surfaces and grain boundaries in Cu thin films and wires. *Phys. Rev. B* **84**, 235423 (2011).
- ⁶⁰X. Huang and W. Zhang, Theoretical study of the thickness dependence of the metal-insulator transition in $\text{Bi}_2\text{Sr}_2\text{Co}_2\text{O}_8$ nanosheets. *Phys. Rev. B* **96**, 035418 (2017).
- ⁶¹T. Zhou and D. Gall, Resistivity scaling due to electron surface scattering in thin metal layers. *Phys. Rev. B* **97**, 165406 (2018).
- ⁶²Y. Yin and A. Tiwari, Understanding the effect of thickness on the thermoelectric properties of $\text{Ca}_3\text{Co}_4\text{O}_9$ thin films. *Sci. Rep.* **11**, 6324 (2021).
- ⁶³Takafumi Ishibe, Yuki Komatsubara, Toranosuke Katayama, Yuichiro Yamashita, Nobuyasu Naruse, Yutaka Mera, Azusa N. Hattori, Hidekazu Tanaka, and Yoshiaki Nakamura, Interface design of transparent thermoelectric epitaxial ZnO/SnO_2 multilayer film for simultaneous realization of low thermal conductivity and high optical transmittance. *Appl. Phys. Lett.* **122**, 041603 (2023).
- ⁶⁴Pablo Darnige, Yohann Thimont, Lionel Presmanes, and Antoine Barnabé, Insights into stability, transport, and thermoelectric properties of transparent p-type copper iodide thin films. *J. Mater. Chem. C*, **11**, 11 (2023).